Imaging small 3D PEC scatterers by SVD and threshold

Aniello Buonanno[*]*, Raffaele Solimene, Rocco Pierri*

Dipartimento di Ingegneria dell'Informazione, Seconda Università di Napoli, I-81031 Aversa, Italy,
[*] Ph.D. Student, e-mail aniello.buonanno@unina2.it

Abstract

The problem of detecting and localizing "small" perfect electric conducting objects from the scattererd far-field is dealt with. By neglecting mutual scattering and representing the scatterers' locations as the support of δ-functions the problem is cast as the inversion of a linear integral operator we tackle by means of the Truncated-Singular Value Decomposition. Scatterers having different sizes are considered for both the cases of mutifrequency and multiview configurations. The performance achievable by the inversion procedure are analyzed against model error and AWG noise.

1.Introduction

In this paper the electromagnetic inverse scattering problem of imaging perfect electric conducting (PEC) Rayleigh objects is dealt with. In particular, the canonical case of PEC spheres having radii much smaller than the wavelength and embedded in the free-space is considered.
Many imaging algorithms have been developed to tackle the problem at hand. Some examples are the time reversal imaging [1], and the time reversal MUSIC algorithm [2-3].
Here we exploit the so-called *linear distributional approach* [4]. First the multiple scattering between the different objects is neglected. However, this does not yield yet a linear relationship between the scattered field data and the unknown scatterers' positions since the latter appear as the argument of the relevant Green's function. Then, the scatterers' positions are represented as the support of Dirac-δ-distributions. This allows to establish a linear integral relationship we invert by means of a Truncated Singular Value Decomposition (TSVD) scheme.
The following configuration is considered. The scatterers, having in general different unknown radii, are assumed to reside within a parallelepiped investigation domain whereas the scattered field is collected over a bounded domain of a sphere concentric to the investigation domain in the far field zone. The incident field is provided by plane waves having fixed direction of incidence and varying frequency (multifrequency/singleview configuration) or fixed frequency and varying direction of incidence (singlefrequency/multiview configuration).
The inversion algorithm is checked against synthetic data which are generated independently from the model used to develop the inversion algorithm by means of the generalized Mie theory in the Rayleigh approximation hypothesis. Finally, also data corrupted by an additive white Gaussian noise are considered.

2. The inversion procedure

Let us consider L PEC small spheres embedded in free space with radius $a_l << \lambda$ (λ being the wavelength) whose centres are located at the points $\underline{r}_l^0 = (x_l, y_l, z_l)$, l = 1, …,L (see Fig. 1). The cluster is illuminated by a plane wave having wave vector $\underline{k} = k(i_X \sin\theta_i \cos\phi_i + i_Y \sin\theta_i \sin\phi_i + i_Z \cos\theta_i)$, with θ_i and ϕ_i being the angles with respect to the z- and the x-axes, respectively, i_x, i_y, i_z are the unit vectors of the Cartesian reference frame and $k = 2\pi/\lambda$ is free-space wavenumber. By considering the incident plane wave of unitary amplitude and TM-polarized, then the field scattered by the ensemble of spheres upon neglecting the mutual scattering is given by

$$E_\theta^s(k,\theta_i,\phi_i,\theta_o,\phi_o) \cong k^3\left[\left(\cos\theta_i\cos\theta_o - \frac{1}{2}\right)\cos(\phi_o-\phi_i) + \sin\theta_i\sin\theta_o\right] \times \sum_{l=1}^{L} a_l^3 \exp[jk(\sin\theta_o\cos\phi_o - \sin\theta_i\cos\phi_i)x_l] \times \exp[jk(\sin\theta_o\sin\phi_o - \sin\theta_i\sin\phi_i)y_l] \times \exp[jk(\cos\theta_o - \cos\theta_i)z_l] \quad (1)$$

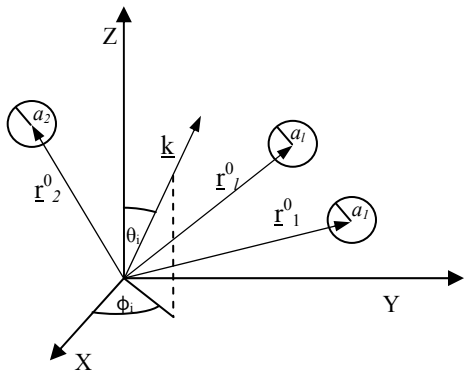

Fig. 1 - Geometry of the problem

where E^s_θ is the far-field along the theta component, θ_o and ϕ_o refer to the observation point and the nonessential spherical factor $\exp[-jkr]/kr$ have been normalized. A similar representation holds also for the ϕ-component. However, it can be shown that it plays a minor role as compared to E^s_θ, hence we do not consider it in the inversion procedure.

Despite the mutual scattering has been neglected, eq. (1) do not give yet a linear relationship from the data and our unknowns. Indeed, the unknown scatterers' positions appear as the arguments of the exponential terms involved in such equation. However, by representing the unknown spheres' positions $\underline{r}^0_l$ as the support of δ-functions we can rewrite eq. (1) as

$$E^s_\theta(k,\theta_i,\phi_i,\theta_o,\phi_o) = f_\theta(k,\theta_i,\phi_i,\theta_o,\phi_o)\times\iiint_D \gamma(x',y',z')\exp[-j(ux'+vy'+wz')]dx'dy'dz' \tag{2}$$

where, $u = k(\sin\theta_i\cos\phi_i - \sin\theta_o\cos\phi_o)$, $v = k(\sin\theta_i\sin\phi_i - \sin\theta_o\sin\phi_o)$, $w = k(\cos\theta_i - \cos\theta_o)$ and f_θ is the multiplicative function appearing in front of the summations in eq. (1), D is the investigation domain where we a priori known that the scatterers reside. Finally,

$$\gamma(\underline{r}') = \sum_{l=1}^{L} a_l^3\,\delta(\underline{r}'-\underline{r}^0_l) \tag{3}$$

accounts for the positions and he radii of scatterers and is the actual unknown of the problem.

Eq. (2) represents the so-called *linear distributional model* upon which the inversion algorithm is based. In particular, to achieve the inversion we adopt the procedure already exploited in [4] for the case of cylindrical scatterers. In particular, such an inversion algorithm is based on a two-step procedure.

In the first step, the distribution is reconstructed by inverting eq. (2) by means of a TSVD procedure. This allows to obtain a stable (with respect to the noise) reconstruction.

In the second step, the total number of the scatterers and their unknown locations are determined as the locus of points where the retrieved distribution achieves its maxima. More in detail, in this second step we introduce a threshold below which the reconstruction is discarded. In particular, we chose a threshold based on the probability of detection of the scatterers, P_D, which in the case of data corrupted by AWG noise is given by

$$P_D = Q\left(\frac{A}{\sqrt{\mathrm{var}_\xi}},\frac{\tau}{\sqrt{\mathrm{var}_\xi}}\right) \tag{4}$$

where $Q(\cdot,\cdot)$ is the Marcum's Q function, τ is the adopted threshold, var_ξ is the variance of the noise process in the reconstruction [5] and A is the amplitude of the reconstruction. Accordingly, eq. (4) returns the probability that the reconstruction having amplitude A is above τ. In particular, if we know the smaller radius we can set A as the maximum amplitude of its reconstruction (when it is alone within the scattering scene) and determine the threshold

so as to have the corresponding P_D equal to 1. Conversely, fixed the threshold τ one can estimate which is the smaller detectable scatterer. Previous discussion does not account for the role of the mutual scattering, its role will discuss in next section.

3.Numerical Reconstructions

In this section, we report some numerical reconstructions obtained by exploiting exact synthetic data corrupted by an Additive White Gaussian Noise (AWGN) η.

A first reconstruction example is reported in Fig. 2 (multifrequency case) and Fig. 3 (multiview case) where a signal-to-noise ratio (SNR) $20\log_{10}\left[\|E_{s\theta}\|/\|\eta\|\right]$ of about 5 dB is employed and an ensemble of nine scatterers having all the same radius (equal to $\lambda_{\max}/20$ and $\lambda/10$, respectively, for the multifrequency and multiview cases) is considered. In particular, the multifrequency reconstruction has been obtained for $\theta_o \in [0,\pi]$rad, $\phi_o \in [\pi,2\pi]$rad and $k \in [2\pi,8\pi]$m^{-1} and with impinging direction along the y-axis, whereas the multiview reconstruction has been obtained for $\theta_i,\theta_o \in [0,\pi]$rad, $\phi_i \in [0,\pi]$, $\phi_o \in [\pi,2\pi]$rad and $k = 4\pi$ m^{-1}. As investigation domain we considered $D = [-x_m.x_m]\times[-y_m.y_m]\times[-z_m.z_m]$, with $x_m = y_m = z_m = \lambda_{\max}$ in the multifrequency case, and $x_m = y_m = z_m = 2\lambda$ for the multiview configuration. The threshold have been chosen according to previous section. As can be seen, in both cases the scatterers are very well localized and discerned.

Further examples are reported in Figs. 4 and 5, where an ensemble of $3\times3\times3$ spherical PEC scatterers uniformly distributed within a box of side $1.4\lambda_{\max}$ and 2.8λ for the mutifrequency and multiview cases are considered. However, now, the scatterers have different radii. In particular, the nine scatterers on the front *x-z* plane (with respect to the incident field) have radius equal to previous case, whereas the spheres on the middle and last *x-z* plane have a radius equal to 80% and 60%, respectively, the one of previous case. As expected, smaller scatterers have a weak reconstruction. Moreover, this is enhanced by the mutual scattering in the multifrequency case (compare Fig. 4 and Fig. 5). Hence, we conclude that from this point of view the multiview configuration works better than the multifrequency one. This is consistent with the study reported in [4] where the case of "thin" scatterers was tackled.

Finally we consider the same case of Figs. 4 and 5, with data corrupted by AWGN as for Fig. 2 and 3 and applying the threshold set accordingly the smaller scatterer (see Figs. 6 and 7). As can be seen, the threshold is helpful in removing spurious artefacts. However, it also removes some of the scatterers (see Fig. 6) in the multifrequency case. This is because, as we pointed out, the estimate of the reconstruction maximum for this configuration is wrong due to the mutual scattering. Once again we conclude that the multiview configuration performs better than the multifrequency one.

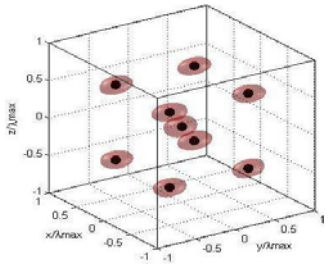

Fig. 2 - Normalized isosurface multifrequency reconstruction of nine scatterers. Actual scatterers (dark-red spheres); reconstructions (pink bubbles). Exact data are employed, AWG noise has been added and threshold is employed.

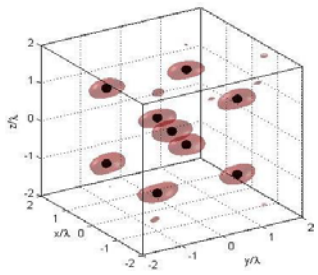

Fig. 3 - Normalized isosurface multiview reconstruction of nine scatterers. Actual scatterers (dark-red spheres); reconstructions (pink bubbles). Exact data are employed, AWG noise has been added and threshold is employed..

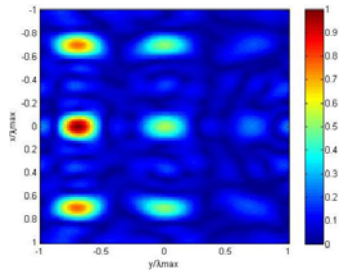

Fig. 4 - Cut view at z = 0 (the other cut views are very similar and are not shown) of normalized multifrequency reconstruction of scatterers. Exact data are employed, no noise has been added and no threshold is employed.

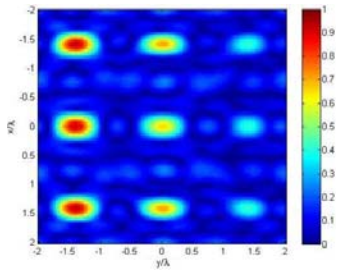

Fig. 5 - Cut view at z = 0 (the other cut views are very similar and are not shown) of normalized multiview reconstruction of scatterers. Exact data are employed, no noise has been added and no threshold is employed.

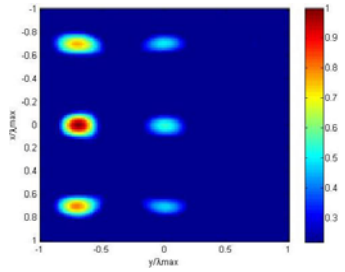

Fig. 6 - The same as Fig. 2 but with AWGN noise and threshold.

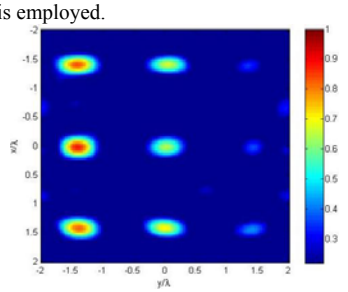

Fig. 7 - The same as Fig. 3 but with AWGN noise and threshold

4.Conclusions

The problem of imaging "small" PEC spheres from the knowledge of the scattered far field has been tackled for multistatic/multifrequency/singleview and multistatic/singlefrequency/multiview reflection mode configurations. A linear TSVD δ-approach supplemented with a threshold procedure has been adopted. The performances achievable by the inversion algorithm have been checked against different radii scatterers in presence of the mutual scattering and the noise by means of numerical reconstructions. The inversion algorithm proven to work well in localizing the small scatterers, also for relatively low SNR. However, it has been shown that the multifrequency configuration is more sensitive than the multiview one to the effect of reciprocal scattering. In particular, in this case, mutual scattering entails a masking effect which makes it more difficult to detect scatterers which are more deeply located along the direction of incidence, specially when they are smaller than the other ones.

5.References

1. D. Liu, G. Kang, L. Li, Y. Chen, S. Vasudevan, W. Joines, Q. H. Liu, J. Krolik, and L. Carin, "Electromagnetic time-reversal imaging of a target in a cluttered environment," *IEEE Trans. Antennas Propag.*, vol. 53, no. 9, pp. 3058–3066, Sep. 2005.

2. E.A. Marengo and F.K. Gruber, "Subspace-based localization and inverse scattering of multiply scattering point targets", *EURASIP Journal on Advances in Signal Processing*, Vol. 2007, Article ID 17342, 16 pages, 2007.

3. Y. Zhong, X. Chen, "MUSIC imaging and electromagnetic inverse scattering of multiple-scattering small anisotropic shperes," *IEEE Trans. Antenn. Prop.*, vol. 55, pp. 3542-3549, 2007.

4. R. Pierri, R. Solimene, A. Liseno, and J. Romano, "Linear distribution imaging of thin metallic cylinders under mutual scattering," *IEEE Trans. Antenn. Prop.*, vol. 53, pp. 3019-3029, 2005.

5. R. Solimene, R. Pierri, "Detection and localization of a slab by a linearlike δ approach," *J. Opt. Soc. Am. A*, vol. 24, pp. 2661-2672, 2007.